Nonlinear Adaptive Speed Control of a Permanent Magnet Synchronous Motor: A Perturbation Estimation Approach

Jian Chen[a], Wei Yao[b,*], Yaxing Ren[c], Lanhong Zhang[a], Lin Jiang[c]

[a]*School of Electrical Engineering, Yancheng Institute of Technology, Yancheng, 224051, China*

[b]*State Key Laboratory of Advanced Electromagnetic Engineering and Technology, School of Electrical and Electronic Engineering, Huazhong University of Science and Technology, Wuhan, 430074, China*

[c]*Department of Electrical Engineering and Electronics, University of Liverpool, Liverpool, L69 3GJ, United Kingdom*

Abstract

This paper presents a nonlinear adaptive control (NAC) scheme for the speed regulation of a permanent magnet synchronous motor (PMSM), based on perturbation estimation and feedback linearizing control. All PMSM system's unknown nonlinearities, parameter uncertainties, and external disturbances including unknown time-varying load torque disturbance, are defined as lumped perturbation terms, which are estimated by designing perturbation observers. The estimates are used to adaptively compensate the real perturbations and achieve adaptive feedback linearizing control of the origi-

*Corresponding author

Email address: w.yao@hust.edu.cn (Wei Yao)

nal nonlinear system. The proposed control scheme does not require accurate system model and full state feedback. Stability of the close-loop system with proposed NAC is investigated via Lyapunov theory, and the effectiveness of proposed NAC scheme is verified through both simulation studies and experimental tests. Both simulation and experimental results show that the proposed NAC can provide less regulation error in speed tracking, better dynamic performance and robustness against parameter uncertainties and load torque disturbance, compared with conventional vector control and load torque estimated based control.
Keywords: permanent magnet synchronous motor (PMSM), nonlinear adaptive control (NAC), perturbation observer, parameter uncertainty, unknown load torque disturbance

1. Introduction

Permanent magnet synchronous motors (PMSMs) are attractive and competitive in AC drive applications due to its self-excitation, high efficiency, high torque-to-inertia and fast dynamic response (Khanchoul, Hilairet and Normand-Cyrot, 2014; Elmas and Ustun, 2008). Traditionally, vector control with proportional-integral loops (VC) is the industrial standard control of the PMSM owing to its decoupling control and simple structure, whose

block diagram has been shown in Fig. 1. However, the VC is not able to guarantee high dynamic performance of a practical PMSM system with inevitable uncertainties such as parameter uncertainties, modeling errors, friction force, and load disturbance (Krishnan, 2001; Yang, Zhang, Liang, Xia, Walker and Zhang, 2018). An effective control strategy plays an important role in providing high performance for the PMSM (Ma, Saeidi, and Kennel, 2014; Feng, Yu and Han, 2013). Therefore, lots of advanced control strategies have been applied to improve control performance of the PMSM, such as model predictive control (Ma, Saeidi, and Kennel, 2014; Chai, Wang and Rogers, 2013; Liu, and Li, 2012), robust control (Lee, Lin and Lin, 2005; Luo, Chen, Ahn and Pi, 2010; Kim, 2017; Mohamed, 2007; Yang, Zhang, Liang, Xia, Walker and Zhang, 2018), sliding mode control (Alsumiri, Li, Jiang and Tang, 2018; Leu, Choi and Jung, 2012; Kim, Son and Lee, 2011), fuzzy control(Cheng and Li, 2011; Choi and Jung, 2013; Choi, Yun and Kim, 2015), backstepping technique(Hamida, Leon and Glumineau, 2017; Kim, Lee and Lee, 2016; Morawiec, 2013), intelligent control (El-Sousy, 2013), and adaptive control (Bifaretti, Iacovone, Rocchi, Tomei and Verrelli, 2012; Verrelli, Tomei, Lorenzani, Migliazza and Immovilli, 2017; Zhou and Wang, 2005; Underwood and Hussain, 2010; Li and Liu, 2009; Jung, Leu, Do, Kim and Choi,

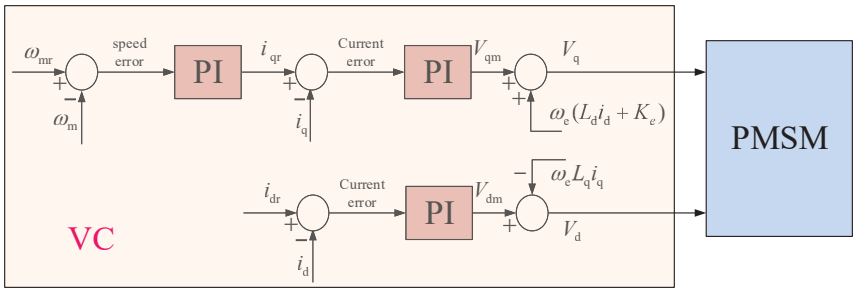

Figure 1: The VC scheme for the PMSM system

2015; Chaoui, Khayamy and Aljarboua, 2017). These nonlinear control techniques have improved the performance of the PMSM system from different aspects.

Recently, observer-based control methods have attracted much attention in improving high robustness against load disturbance and parameter uncertainties of the PMSM, which have become one of the most commonly used schemes in AC machine drives (Yang, Chen, Li, Guo and Yan, 2017; Lu, 2008). Although observer based control methods proposed in (Solsona, Valla and Muravchik, 1996, 2000; Kim and Youn, 2002; Sira-ramirez, Linares-Flores, Garcia-Rodriguez and Contreras-Ordaz, 2014; Zhu, Dessaint, Akhrif and Kaddouri, 2000; Linares-Flores, Garcia-Rodriguez, Sira-Ramirez and Ramirez-Cardenas, 2015; Preindl and Bolognani, 2013) can provide satisfactory performance under load torque disturbance, the performances of the

observers relying on accurate system model or parameters will degrade with parameter uncertainties. In (Solsona, Valla and Muravchik, 1996, 2000; Zhu, Dessaint, Akhrif and Kaddouri, 2000; Preindl and Bolognani, 2013), model-based reduced-order nonlinear observer, extended-order nonlinear observer (ENO), linear extended observer and state-observer based controllers have been proposed to improve the robustness against slowly varying load torque disturbance. However, these three observer based control methods show sensitivity to parameter variations. In (Kim and Youn, 2002; Sira-ramirez, Linares-Flores, Garcia-Rodriguez and Contreras-Ordaz, 2014; Linares-Flores, Garcia-Rodriguez, Sira-Ramirez and Ramirez-Cardenas, 2015), reduced-order observer, linear extended high-gain observer and linear extended state observer have been used to achieve satisfactory performance in the presence of load torque disturbance and provide high robustness against certain parameter uncertainties. However, some system parameters are still required to be exactly known.

To improve control performance of the observer-based controllers depending on exactly known system parameters, observer-based control methods independent of accurate system parameters proposed in (Xu, Jiang and Mu, 2016; Son, Kim, Choi and Shim, 2015; Zhang, Sun, Zhao and Sun, 2013;

Su, Zheng, and Duan, 2005; Tami, Boutat, Zheng, Kratz and Gouri, 2017; Niu, Zhang, and Li, 2017; Zhang and Li, 2017; Feng, Yu and Han, 2013; Li, Zhou and Yu, 2013) not only provide high robustness against load torque disturbance, but also improve the control performance with system parameter uncertainties. In (Zhang and Li, 2017; Feng, Yu and Han, 2013), an extended sliding-mode observer and a terminal sliding-mode observer have been proposed to estimate mechanical parameter and load torque, respectively. Since the electrical parameters can be easily measured using instruments or sensors compared with the mechanical parameters, they focus on the estimation of the mechanical parameters. Nevertheless, electrical parameters are time-varying in most cases due to varying temperature, the effects of cross saturation and magnetic saturation. These electrical parameters are difficult to be accurately measured during operation period (Liu and Zhu, 2014; Yan, Yang, Sun, Zhang, Li and Yu, 2018; Jiang, Xu, Mu, and Liu, 2018). In (Xu, Jiang and Mu, 2016), a sliding mode control in combination with a disturbance observer has been introduced to solve time-varying parameter and disturbances. However, the parameters selection of the controllers and observers are complex and time consuming, and it also lacks of parameter uncertainties test results. Although disturbance observer methods in (Zhang,

Sun, Zhao and Sun, 2013; Li, Zhou and Yu, 2013) have been developed to optimize the control performance of the PMSM system with disturbance and uncertainties, parameter uncertainties test results have not shown. In (Tami, Boutat, Zheng, Kratz and Gouri, 2017; Niu, Zhang, and Li, 2017), nonlinear disturbance observer and extended nonlinear observer have been applied to estimate uncertain parameters and unknown load torque, but experimental results have not shown. An automatic disturbances rejection controller design scheme using extended state observer has already been investigated for high-performance robust motion control of the PMSM, which focuses on position regulation (Su, Zheng, and Duan, 2005). In (Son, Kim, Choi and Shim, 2015), a new practical control structure using dual proportional-integral (PI) observers has been proposed to maintain nominal performance against parameter uncertainties as well as slowly varying disturbance. In (Yan, Yang, Sun, Zhang, Li and Yu, 2018; Jiang, Xu, Mu, and Liu, 2018; Zhang, Hou and Mei, 2017), a comprehensive disturbance observer, a high-order sliding mode observer, and an adaptive stator current and disturbance observer have been employed for improving the control performance of the PMSM system with high robustness against disturbance and parameter uncertainties. In addition to aforementioned observer-based control methods, a nonlinear adaptive

control using high-gain states and perturbation observer (HGO) has been successfully applied in different fields (Chen, Jiang, Yao and Wu, 2014; Jiang, Wu, and Wen, 2004), which can guarantee satisfactory system performance with parameter or model uncertainties and load disturbance.

In this paper, a high-gain observer-based nonlinear adaptive controller (HGO-NAC) of the PMSM is developed to track mechanical rotation speed and provide high robustness against system parameter uncertainties and unknown fast varying load torque disturbance. The idea of the HGO-NAC is based on the state and perturbation estimation and feedback linearizing control. In the design of the HGO-NAC, by defining lumped perturbation terms to present coupling nonlinear dynamics, parameter uncertainties, unknown disturbances, and interactions among subsystems, perturbation observers are designed to estimate the perturbations, which are used to compensate the real perturbations and realize an adaptive linearizing of the original nonlinear system, without requiring the accurate system model and full state measurements, and ignoring any system nonlinearities and unknown dynamics. A nonlinear controller with an ENO (ENO-NC) based on the control method proposed in (Solsona, Valla and Muravchik, 2000) is used for comparing with the proposed HGO-NAC. In the ENO-NC design, the mechanical rotation

speed, rotor position, and stator current are required to be measured, only the unknown load torque and its derivative are estimated by the ENO. The proposed HGO-NAC will be compared with the ENO-NC and VC under different conditions. The effectiveness of the proposed HGO-NAC is verified by both simulation and experimental results.

The main differences between the current paper and previous work (Chen, Jiang, Yao and Wu, 2014) can be listed as follows,

1) The nonlinear adaptive controller (NAC) of a full-rated converter wind-turbine proposed in previous work (Chen, Jiang, Yao and Wu, 2014) is only verified by simulation studies, while the nonlinear adaptive speed controller of PMSM proposed in this paper is verified by not only simulation studies but also hardware-in-loop experimental studies.

2) In previous work (Chen, Jiang, Yao and Wu, 2014), the proposed NAC is only compared with conventional vector controller (VC) with proportional-integral loops and feedback linearizing control (FLC), while the nonlinear adaptive speed controller of PMSM proposed in this paper is compared with not with the conventional VC but also a series of perturbation observer-base controller including a nonlinear controller with an extended-order nonlinear observer (ENO-NC), active disturbance rejection control (ADRC), sliding-

mode states and perturbation observer based NAC (SMO-NAC).

3) The system output references in the previous work (Chen, Jiang, Yao and Wu, 2014)are both constant, while system output reference in this paper is rotation speed reference and could be constant or timevarying. Moreover, this paper considers the time-varying load torque disturbance and the mechanical rotation speed variation simultaneously, which poses higher requirements for the control system.

The rest of this paper is organized as follows. In Section 2, the PMSM model is briefly recalled. The HGO-NAC designing for the PMSM and the stability analysis of closed-loop system are presented in Section 3. Sections 4 and 5 respectively carry out simulation and experimental results to verify the performance of the proposed HGO-NAC, compared with the ENO-NC and VC. Finally, conclusions are drawn in Section 6.

2. Model of Permanent Magnet Synchronous Motor

In this Section, the state-space PMSM model in d-q reference frame is briefly recalled, which can be obtained as (Lin, Liu and Yang, 2008)

$$\dot{x} = f(x) + g_1(x)u_1 + g_2(x)u_2 \tag{1}$$

where

$$
\begin{aligned}
f(x) &= \begin{bmatrix} -\frac{R_\mathrm{s}}{L_\mathrm{d}} i_\mathrm{d} + \frac{\omega_\mathrm{e} L_\mathrm{q}}{L_\mathrm{d}} i_\mathrm{q} \\ -\frac{R_\mathrm{s}}{L_\mathrm{q}} i_\mathrm{q} - \frac{1}{L_\mathrm{q}} \omega_\mathrm{e} (L_\mathrm{d} i_\mathrm{d} + K_e) \\ \frac{1}{J}(T_\mathrm{e} - T_\mathrm{L} - D\omega_\mathrm{m}) \end{bmatrix}, \\
g_1(x) &= [\tfrac{1}{L_\mathrm{d}} \quad 0 \quad 0]^\mathrm{T}, \\
g_2(x) &= [0 \quad \tfrac{1}{L_\mathrm{q}} \quad 0]^\mathrm{T}, \\
x &= [i_\mathrm{d} \quad i_\mathrm{q} \quad \omega_\mathrm{m}]^\mathrm{T}, \\
u &= [u_1, u_2]^T = [V_\mathrm{d}, V_\mathrm{q}]^T, \\
y &= [y_1, y_2]^T = [h_1(x), h_2(x)]^T = [i_\mathrm{d}, \omega_\mathrm{m}]^T
\end{aligned}
$$

where, $x \in R^3$, $u \in R^2$ and $y \in R^2$ are state vector, input vector and output vector, respectively; $f(x)$, $g(x)$ and $h(x)$ are smooth vector fields. V_d and V_q are the stator voltages in the d-q axis, i_d and i_q are the stator currents in the d-q axis, R_s is the stator resistance, L_d and L_q are d-q axis inductances, K_e is the field flux given by the magnets, p is the number of pole pairs, J is the inertia of the drive train, ω_m is the mechanical rotation speed, $\omega_\mathrm{e}(= p\omega_\mathrm{m})$ is the electrical generator rotation speed, D is the viscous friction coefficient, T_e is the electromagnetic torque, and T_L is the load torque disturbance, which is assumed unknown.

The electromagnetic torque is expressed as (Lin, Liu and Yang, 2008)

$$T_{\mathrm{e}} = \frac{3}{2} p[(L_{\mathrm{d}} - L_{\mathrm{q}}) i_{\mathrm{d}} i_{\mathrm{q}} + i_{\mathrm{q}} K_e] \tag{2}$$

3. Nonlinear adaptive control

In this Section, the HGO-NAC designing for the PMSM and the stability analysis of closed-loop system are presented. The nonlinear adaptive control based on perturbation observer proposed in (Chen, Jiang, Yao and Wu, 2014; Jiang, Wu, and Wen, 2004) will be used. A multi-input multi-output (MIMO) system is transformed as interacted subsystems via input/output linearization at first. Then for each subsystem, a perturbation term is defined to include all subsystem nonlinearities, interactions between subsystems and uncertainties. A fictitious state introduced to represent the perturbation and an extended-order high-gain observer is designed to estimate the perturbation and system states, based on the measured system outputs. The estimates of perturbations and system states are used to realize an output feedback and adaptive linearizing control of the original nonlinear system.

3.1. Input-Output Linearization

In this Sub-section, the PMSM system is transformed as interacted subsystems via input-output linearization at first. For system (1), choose the output of the first subsystem as $y_1 = h_1(x) = i_\mathrm{d}$ and output of the second subsystem as $y_2 = h_2(x) = \omega_\mathrm{m}$, we have

$$\begin{bmatrix} y_1^{(1)} \\ y_2^{(2)} \end{bmatrix} = \begin{bmatrix} F_1(x) \\ F_2(x) \end{bmatrix} + B(x) \begin{bmatrix} u_1 \\ u_2 \end{bmatrix} \tag{3}$$

where

$$F_1(x) = \frac{1}{L_\mathrm{d}}(-i_\mathrm{d}R_\mathrm{s} + \omega_\mathrm{e}L_\mathrm{q}i_\mathrm{q}) \tag{4}$$

$$\begin{aligned} F_2(x) = & -\frac{3p}{2JL_\mathrm{q}}[K_e + (L_\mathrm{d} - L_\mathrm{q})i_\mathrm{d}](L_\mathrm{d}\omega_\mathrm{e}i_\mathrm{d} \\ & + R_\mathrm{s}i_\mathrm{q} + \omega_\mathrm{e}K_e) + \frac{3pi_\mathrm{q}(L_\mathrm{d} - L_\mathrm{q})}{2JL_\mathrm{d}}(-R_\mathrm{s}i_\mathrm{d} \\ & + L_\mathrm{q}\omega_\mathrm{e}i_\mathrm{q}) - \frac{1}{J}\frac{dT_\mathrm{L}}{dt} \\ & - \frac{D}{J^2}[\frac{3p}{2}(L_\mathrm{d} - L_\mathrm{q})i_\mathrm{d}i_\mathrm{q} + \frac{3p}{2}i_\mathrm{q}K_e - T_\mathrm{L} \\ & - D\omega_\mathrm{m}) \end{aligned} \tag{5}$$

$$B(x) = \begin{bmatrix} B_1(x) \\ B_2(x) \end{bmatrix} = \begin{bmatrix} \frac{1}{L_\mathrm{d}} & 0 \\ \frac{3pi_\mathrm{q}(L_\mathrm{d}-L_\mathrm{q})}{2JL_\mathrm{d}} & \frac{3p[K_e+(L_\mathrm{d}-L_\mathrm{q})i_\mathrm{d}]}{2JL_\mathrm{q}} \end{bmatrix} \tag{6}$$

For a practical PMSM system, the values of parameters $p, K_e, J, L_\mathrm{d}, L_\mathrm{q}$ should be all non-zero. The determinant of B_x ($det[B(x)] = \frac{3p[K_e+(L_\mathrm{d}-L_\mathrm{q})i_\mathrm{d}]}{2JL_\mathrm{d}L_\mathrm{q}} \neq 0$) should be non-zero, that is, $B(x)$ is nonsingular for all nominal operation points. The system (1) has relative degree $r_i = [1 \quad 2]$.

The feedback linearization control of system (1) is obtained as

$$\begin{pmatrix} u_1 \\ u_2 \end{pmatrix} = B(x)^{-1} \left(\begin{pmatrix} -F_1(x) + v_1 \\ -F_2(x) + v_2 \end{pmatrix} \right) \tag{7}$$

$$B(x)^{-1} = \begin{pmatrix} L_\mathrm{d} & 0 \\ -\frac{i_\mathrm{q}L_\mathrm{q}(L_\mathrm{d}-L_\mathrm{q})}{K_e+(L_\mathrm{d}-L_\mathrm{q})i_\mathrm{d}} & \frac{2JL_\mathrm{q}}{3p[K_e+(L_\mathrm{d}-L_\mathrm{q})i_\mathrm{d}]} \end{pmatrix} \tag{8}$$

And the original system is linearized as

$$\begin{pmatrix} \dot{y}_1 \\ \ddot{y}_2 \end{pmatrix} = \begin{pmatrix} v_1 \\ v_2 \end{pmatrix} \tag{9}$$

$$v_1 = \dot{y}_{1\mathrm{r}} + k_{11}(y_{1\mathrm{r}} - y_1) \tag{10}$$

$$v_2 = \ddot{y}_{2\mathrm{r}} + k_{21}(y_{2\mathrm{r}} - y_2) + k_{22}(\dot{y}_{2\mathrm{r}} - \dot{y}_2) \tag{11}$$

where, v_1 and v_2 are inputs of linear systems, k_{11}, k_{21} and k_{22} are gains of linear controller, $y_{1\mathrm{r}}$ and $y_{2\mathrm{r}}$ are the desired output references. Define $e_1 = y_{1\mathrm{r}} - y_1$ and $e_2 = y_{2\mathrm{r}} - y_2$ as track errors, the error dynamics are

$$\dot{e}_1 + k_{11}e_1 = 0 \tag{12}$$

$$\ddot{e}_2 + k_{22}\dot{e}_2 + k_{21}e_2 = 0 \tag{13}$$

3.2. Definition of Perturbation and Fictitious State

In this Sub-section, for each subsystem, a perturbation term is defined to include all subsystem nonlinearities, interactions between subsystems and uncertainties. Assume all nonlinearities of system (3) are unknown, and define perturbation terms as

$$\begin{bmatrix} \Psi_1 \\ \Psi_2 \end{bmatrix} = \begin{bmatrix} F_1(x) \\ F_2(x) \end{bmatrix} + (B(x) - B_0) \begin{bmatrix} u_1 \\ u_2 \end{bmatrix} \tag{14}$$

where $\Psi_{1,2}$ are the perturbation terms, and $B_0 = B(x)|_{x=x(0)}$ is the nominal control gain and expressed as

$$B_0 = \begin{bmatrix} \frac{1}{L_{\mathrm{d}0}} & 0 \\ \frac{3pi_{\mathrm{q}}(L_{\mathrm{d}0}-L_{\mathrm{q}0})}{2J_0L_{\mathrm{d}0}} & \frac{3p[K_{e0}+(L_{\mathrm{d}0}-L_{\mathrm{q}0})i_{\mathrm{d}}]}{2J_0L_{\mathrm{q}0}} \end{bmatrix} \tag{15}$$

where $L_{\mathrm{d}0}$, $L_{\mathrm{q}0}$, J_0 and K_{e0} are respectively the nominal values of L_{d}, L_{q}, J and K_e.

Then system (3) can be rewritten as

$$\begin{bmatrix} y_1^{(1)} \\ \\ y_2^{(2)} \end{bmatrix} = \begin{bmatrix} \Psi_1 \\ \\ \Psi_2 \end{bmatrix} + B_0 \begin{bmatrix} u_1 \\ \\ u_2 \end{bmatrix} \tag{16}$$

For the first subsystem, defining state variables as $z_{11} = y_1$, and a fictitious state to represent the perturbation $z_{12} = \Psi_1$, the first subsystem can be represented as

$$S1 : \begin{cases} z_{11} &= y_1 \\ \dot{z}_{11} &= z_{12} + B_{0_1} u \\ \dot{z}_{12} &= \dot{\Psi}_1 \end{cases} \tag{17}$$

where B_{0_1} is the first row of the B_0, $B_{0_{ij}}$ is the i^{th} row j^{th} column element of the B_0.

For the second subsystem, defining state variables as $z_{21} = y_2$ and $z_{22} = y_2^{(1)}$, and a fictitious state to represent the perturbation $z_{23} = \Psi_2$, the second subsystem can be represented as

$$S2 : \begin{cases} z_{21} &= y_2 \\ \dot{z}_{21} &= z_{22} \\ \dot{z}_{22} &= z_{23} + B_{0_2} u \\ \dot{z}_{23} &= \dot{\Psi}_2 \end{cases} \tag{18}$$

where B_{0_2} is the second row of the B_0.

For subsystems (17) and (18), several types of perturbation observers, such as sliding mode observer, high gain observer and linear Luenberger observer, have been proposed (Chen, Jiang, Yao and Wu, 2014; Jiang, Wu, and Wen, 2004; Jiang and Wu, 2002). This paper uses high gain observer proposed in (Chen, Jiang, Yao and Wu, 2014), while other observers can be designed similarly.

3.3. Design of States and Perturbation Observer

In this Sub-section, a fictitious state introduced to represent the perturbation and an extended-order high-gain observer is designed to estimate the perturbation and system states, based on the measured system outputs.

When the system outputs y_1 and y_2 are available, a second-order and a third-order states and perturbation observers (SPOs) are designed to estimate states and perturbations of the subsystems as

$$S1: \begin{cases} \dot{\hat{z}}_{11} &= \hat{z}_{11} + l_{11}(z_{11} - \hat{z}_{11}) + B_{0_1} u \\ \dot{\hat{z}}_{12} &= l_{12}(z_{11} - \hat{z}_{11}), \end{cases} \tag{19}$$

$$S2: \begin{cases} \dot{\hat{z}}_{21} &= \hat{z}_{22} + l_{21}(z_{21} - \hat{z}_{21}) \\ \dot{\hat{z}}_{22} &= \hat{z}_{23} + l_{22}(z_{21} - \hat{z}_{21}) + B_{0_2} u \\ \dot{\hat{z}}_{23} &= l_{23}(z_{21} - \hat{z}_{21}), \end{cases} \tag{20}$$

where $\hat{z}_{11}$, $\hat{z}_{12}$, $\hat{z}_{21}$, $\hat{z}_{22}$ and $\hat{z}_{23}$ are the estimations of z_{11}, z_{12}, z_{21}, z_{22} and z_{23}, respectively, and l_{11}, l_{12}, l_{21}, l_{22}, l_{23} are gains of the observers, which are designed as

$$l_{ij} = \frac{\alpha_{ij}}{\epsilon_i^j} \tag{21}$$

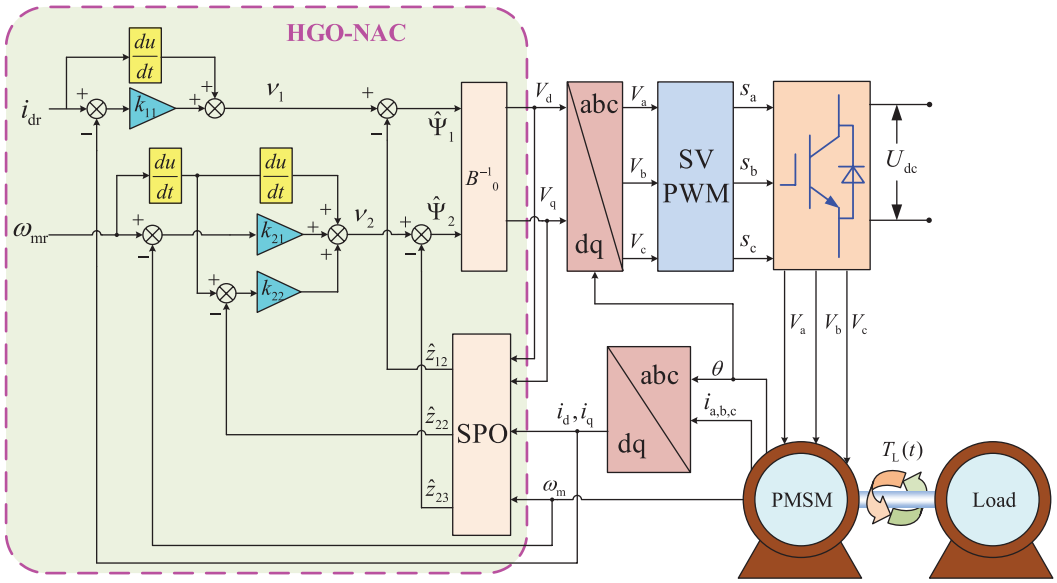

Figure 2: The HGO-NAC scheme for the PMSM system

where $i = 1, 2$; $j = 1, \cdots, r_i + 1$, ϵ_i is a scalar chosen to be within (0,1) for representing times of the time-dynamics between the observer and the real system, and parameters α_{ij} are chosen so that the roots of

$$s^{r_i+1} + \alpha_{i1} s^{r_i} + \cdots + \alpha_{ir_i} s + \alpha_{i(r_i+1)} = 0 \tag{22}$$

are in the open left-half complex plane.

Remark1. It should be mentioned that during the design procedure, ϵ_i used in SPOs (19) and (20) are required to be some relatively small positive constants only, and the performance of SPOs is not very sensitive to

the observer gains, which are determined based on the upper bound of the derivative of perturbation.

3.4. Design of Nonlinear Adaptive Controller

In this Sub-section, the estimates of perturbations and system states are used to realize an output feedback and adaptive linearizing control of the original nonlinear system.

By using the estimated perturbation to compensate the real perturbation, control laws for both subsystems are obtained as:

$$\begin{bmatrix} u_1 \\ u_2 \end{bmatrix} = B_0^{-1} \left[\begin{bmatrix} -\hat{z}_{12} \\ -\hat{z}_{23} \end{bmatrix} + \begin{bmatrix} v_1 \\ v_2 \end{bmatrix} \right] \tag{23}$$

where $v_{1,2}$ is defined as

$$\begin{cases} v_1 &= k_{11}(z_{11\mathrm{r}} - z_{11}) + \dot{z}_{11\mathrm{r}} \\ v_2 &= \ddot{z}_{21\mathrm{r}} + k_{21}(z_{21\mathrm{r}} - z_{21}) \\ & \quad +k_{22}(\dot{z}_{21\mathrm{r}} - \hat{z}_{22}) \end{cases} \tag{24}$$

where z_{11r} and z_{21r} are the references of z_{11} and z_{21}, respectively.

The final control law represented by physical variables, such as currents, inductance, total inertia, field flux and mechanical rotation speed, are given

as follows:

$$\begin{cases} u_1 = L_{\mathrm{d0}}[k_{11}(i_{\mathrm{dr}} - i_{\mathrm{d}}) + \dot{i}_{\mathrm{dr}} - \hat{z}_{12}] \\ u_2 = -\frac{i_{\mathrm{q}} L_{\mathrm{q0}}(L_{\mathrm{d0}} - L_{\mathrm{q0}})}{K_{e0} + (L_{\mathrm{d0}} - L_{\mathrm{q0}}) i_{\mathrm{d}}}[k_{11}(i_{\mathrm{dr}} - i_{\mathrm{d}}) + \dot{i}_{\mathrm{dr}} - \hat{z}_{12}] \\ \qquad + \frac{2 J_{\mathrm{tot0}} L_{\mathrm{q0}}}{3p[K_{e0} + (L_{\mathrm{d0}} - L_{\mathrm{q0}}) i_{\mathrm{d}}]}[k_{21}(\omega_{\mathrm{mr}} - \omega_{\mathrm{m}}) \\ \qquad + k_{22}(\dot{\omega}_{\mathrm{mr}} - \hat{z}_{22}) + \ddot{\omega}_{\mathrm{mr}} - \hat{z}_{23}] \end{cases} \tag{25}$$

Note that in the controller design, the proposed HGO-NAC only requires the nominal parameter values of L_{d0}, L_{q0}, K_{e0} and J_0, and the measurements of currents and ω_{m}.

To clearly illustrate the principle of the proposed HGO-NAC for the PMSM system, a block diagram is shown in Fig. 2.

The following assumptions are made in (Jiang and Wu, 2002; Jiang, Wu, and Wen, 2004; Youcef and Wu, 1992; Wu, Jiang and Wen, 2004; Yang, Jiang, Yao and Wu, 2015; Yang, Yu, Shu, Dong and Jiang, 2018).

Assumption 1: Input gain B(x) and its derivative are bounded by $0 < B_1 \leq B(x) \leq B_2$, $|\dot{B}(x)| \leq B_3$, where B_i, $i = 1, 2, 3$ are finite constants [for convenience we assume that $B(x) > 0$]. $B(0)$ is chosen to satisfy: $|B(x)/B(0) - 1| \leq \theta < 1$, where θ is a positive constant. The control u is assumed to be bounded but big enough for the purpose of perturbation

cancellation.

Assumption 2: The perturbation $\Psi_i(x,t)$ and its derivative $\dot{\Psi}_i(x,t)$ are locally Lipschitz in their arguments and bounded over the domain of interest.

3.5. Stability Analysis of Closed-Loop System

This subsection analyzes the stability of the closed-loop system equipped with the HGO-NAC designed in the previous section.

At first, both the estimation error system and the tracking error system are obtained. On one hand, by defining estimation errors $\varepsilon_{11} = z_{11} - \hat{z}_{11}$, $\varepsilon_{12} = z_{12} - \hat{z}_{12}$, $\varepsilon_{21} = z_{21} - \hat{z}_{21}$, $\varepsilon_{22} = z_{22} - \hat{z}_{22}$, $\varepsilon_{23} = z_{23} - \hat{z}_{23}$, subtracting (19) from (17) and subtracting (20) from (18), the following estimation error system yields:

$$\dot{\varepsilon}_i = A_i \varepsilon_i + \eta_i \tag{26}$$

where

$$\varepsilon_i = \begin{bmatrix} \varepsilon_{11} \\ \varepsilon_{12} \\ \varepsilon_{21} \\ \varepsilon_{22} \\ \varepsilon_{23} \end{bmatrix}, \qquad \eta_i = \begin{bmatrix} 0 \\ \dot{\Psi}_1 \\ 0 \\ 0 \\ \dot{\Psi}_2 \end{bmatrix},$$

$$A_i = \begin{bmatrix} -l_{11} & 1 & 0 & 0 & 0 \\ -l_{12} & 0 & 0 & 0 & 1 \\ 0 & 0 & -l_{21} & 1 & 0 \\ 0 & 0 & -l_{22} & 0 & 1 \\ 0 & 0 & -l_{23} & 0 & 0 \end{bmatrix} \tag{27}$$

On the other hand, define the tracking errors as $e_{11} = y_{1\mathrm{r}} - z_{11}$, $e_{21} = y_{2\mathrm{r}} - z_{21}$ and $e_{22} = \dot{y}_{2\mathrm{r}} - z_{22}$. It follows from (18) that $\dot{e}_{21} = e_{22}$.

And, it follows from (16), (23) and (24) that

$$\begin{bmatrix} \dot{e}_{11} \\ \dot{e}_{22} \end{bmatrix} = - \begin{bmatrix} k_{11}(e_{11} + \varepsilon_{11}) + \varepsilon_{12} \\ k_{21}(e_{21} + \varepsilon_{21}) + k_{22}(e_{22} + \varepsilon_{22}) + \varepsilon_{23} \end{bmatrix} \tag{28}$$

Thus, the tracking error system can be summarized as

$$\dot{e}_i = M_i e_i + \vartheta_i \tag{29}$$

where

$$e_i = \begin{bmatrix} e_{11} \\ e_{21} \\ e_{22} \end{bmatrix}, \qquad \vartheta_i = \begin{bmatrix} -\xi_1 \\ 0 \\ -\xi_2 \end{bmatrix},$$

$$M_i = \begin{bmatrix} -k_{11} & 0 & 0 \\ 0 & 0 & 1 \\ 0 & -k_{21} & -k_{22} \end{bmatrix} \tag{30}$$

with $\xi_1 = \varepsilon_{12}$ and $\xi_2 = k_{21}\varepsilon_{21} + k_{22}\varepsilon_{22} + \varepsilon_{23}$ being the lumped estimation error.

The stability analysis of the closed-loop control system is transformed into globally uniformly ultimately bounded summarized.

Theorem 1. Consider the PMSM system (3) equipped the proposed HGO-NAC (25) with two SPOs (19) and (20). If the real perturbation $\Psi_i(x,t)$ defined in (14) satisfies

$$\|\Psi_i(x,t)\| \leq \gamma_1 \tag{31}$$

then both the estimation error system (26) and the tracking error system (29) are, i.e.,

$$\|\varepsilon_i(t)\| \leq 2\gamma_1\|P_1\|, \|e_i(t)\| \leq 4\gamma_1\|K_i\|\|P_1\|\|P_2\|, \forall t \geq T \tag{32}$$

where P_i, $i = 1, 2$ are respectively the feasible solutions of Riccati equations

$A_i^{\mathrm{T}} P_1 + P_1 A_i = -I$ and $M_i^{\mathrm{T}} P_2 + P_2 M_i = -I$; and $\|K_i\|$ is a constant related to k_{11}, k_{21} and k_{22}.

Proof. For the estimation error system (26), consider the following Lyapunov function:

$$V_{i1}(\varepsilon_i) = \varepsilon_i^{\mathrm{T}} P_1 \varepsilon_i \tag{33}$$

The high gains of SPOs (19) and (20) are determined by requiring (22) holds, which means A_i is Hurwitz. One can find a feasible positive definite solution, P_1, of Riccati equation $A_i^{\mathrm{T}} P_1 + P_1 A_i = -I$. Calculating the derivative of $V_{i1}(\varepsilon_i)$ along the solution of system (26) and using (31) to yield

$$\begin{aligned} \dot{V}_{i1}(\varepsilon_i) &= \varepsilon_i^{\mathrm{T}}(A_i^{\mathrm{T}} P_1 + P_1 A_i)\varepsilon_i + \eta_i^{\mathrm{T}} P_1 \varepsilon_i + \varepsilon_i^{\mathrm{T}} P_1 \eta_i \\ &\leq -\|\varepsilon_i\|^2 + 2\|\varepsilon_i\| \cdot \|\eta_i\| \cdot \|P_1\| \\ &\leq -\|\varepsilon_i\|(\|\varepsilon_i\| - 2\gamma_1 \|P_1\|) \end{aligned} \tag{34}$$

Then $\dot{V}_{i1}(\varepsilon_i) \leq 0$ when $\|\varepsilon_i\| \geq 2\gamma_1 \|P_1\|$. Thus there exists $T_1 > 0$, which can lead to

$$\|\varepsilon_i(t)\| \leq \gamma_2 = 2\gamma_1 \|P_1\|, \forall t \geq T_1 \tag{35}$$

For tracking error system (29), one can find that $\|\vartheta_i\| \leq \|K_i\|\gamma_2$ with $\|K_i\|$

based on $\|\varepsilon_i(t)\| \leq \gamma_2$. Consider the Lyapunov function $V_{i2}(e_i) = e_i^{\mathrm{T}} P_2 e_i$. Similarly, one can prove that, there exists an instant, T_1, the following holds

$$\|e_i(t)\| \leq 2\|K_i\|\gamma_2\|P_2\| \leq 4\gamma_1\|K_i\|\|P_1\|\|P_2\|, \forall t \geq \bar{T}_1 \tag{36}$$

Using (35) and (36) and setting $T = \max\{T_1, \bar{T}_1\}$ lead to (32).

Moreover, if $\Psi_i(x,t)$ and $\dot{\Psi}_i(x,t)$ are locally Lipschitz in their arguments, it will guarantee the exponential convergence of the observation error (Jiang and Wu, 2002) and closed-loop tracking error into

$$\lim_{t\to\infty} \varepsilon_i(t) = 0 \quad \text{and} \quad \lim_{t\to\infty} e_i(t) = 0 \tag{37}$$

After the states ω_{m} and i_{d} and their derivatives are stable that controlled by HGO-NAC. The parameter variation is considered in the error system in (26) and (29), and the error system is proved as converged to zero in (37). This guarantees that the estimated perturbations track the extended states defined in (14), which includes the uncertainties affected by the parameter variations and disturbances, and compensates the control input in (23). Then the linearized subsystems in (17) and (18) are independent of the parameters and disturbances.

Remark2. The perturbation and its derivative are assumed to locally bounded as described in **Assumption 2**. The existence of these bounds can be shown in the following analysis. The perturbation and its derivative can be represented as

$$
\begin{aligned}
\Psi_1 &= F_1(x) + \frac{B_{11}(x) - B_{0_{11}}}{B_{11}(x)}[k_{11}(z_{11r} - z_{11}) + z_{12} - \hat{z}_{12}] \\
&= F_1(x) + \frac{B_{11}(x) - B_{0_{11}}}{B_{11}(x)}(k_{11}e_{11} + \varepsilon_{12}) \\
\dot{\Psi}_1 &= \dot{F}_1(x) + \frac{B_{11}(x) - B_{0_{11}}}{B_{0_{11}}}(-\dot{\Psi}_1 + k_{11}\dot{e}_{11} - \dot{\varepsilon}_{12}) \\
&= \dot{F}_1(x) + \frac{B_{11}(x) - B_{0_{11}}}{B_{0_{11}}}(k_{11}\dot{e}_{11} + l_{12}\varepsilon_{11}) \\
\Psi_2 &= F_2(x) + B_{21}(x)^{-1}(B_{21}(x) - B_{0_{21}})[k_{11}(z_{11r} - z_{11}) + z_{12} - \hat{z}_{12}] + \\
&\quad B_{22}(x)^{-1}(B_{22}(x) - B_{0_{22}})[k_{21}(z_{21r} - z_{21}) + k_{22}(\dot{z}_{21r} - z_{22}) + z_{23} - \hat{z}_{23}] \\
&= F_2(x) + B_{21}(x)^{-1}(B_{21}(x) - B_{0_{21}})(k_{11}e_{11} + \varepsilon_{12}) + \\
&\quad B_{22}(x)^{-1}(B_{22}(x) - B_{0_{22}})(k_{21}e_{21} + k_{22}e_{22} + \varepsilon_{23}) \\
\dot{\Psi}_2 &= \dot{F}_2(x) + \frac{B_{21}(x) - B_{0_{21}}}{B_{0_{21}}}(-\dot{\Psi}_1 + k_{11}\dot{e}_{11} - \dot{\varepsilon}_{12}) + \\
&\quad \frac{B_{22}(x) - B_{0_{22}}}{B_{0_{22}}}(-\dot{\Psi}_2 + k_{21}\dot{e}_{21} + k_{22}\dot{e}_{22} - \dot{\varepsilon}_{23}) \\
&= \dot{F}_2(x) + \frac{B_{21}(x) - B_{0_{21}}}{B_{0_{21}}}(k_{11}\dot{e}_{11} + l_{12}\varepsilon_{11}) + \\
&\quad \frac{B_{22}(x) - B_{0_{22}}}{B_{0_{22}}}(k_{21}\dot{e}_{21} + k_{22}\dot{e}_{22} + l_{13}\varepsilon_{21})
\end{aligned}
$$

Considering **Assumption 1**, we have

$$
\begin{aligned}
\mid \Psi_1 \mid &\leq \frac{1}{1-\theta_1} \mid F_1(x) \mid + \frac{\theta_1}{1+\theta_1}(\parallel k_{11} \parallel\parallel e_{11} \parallel + \mid \varepsilon_{12} \mid) \\
\mid \dot{\Psi}_1 \mid &\leq \mid \dot{F}_1(x) \mid + \mid B_{11}(x) \mid\mid u_1 \mid + \theta_1(\parallel k_{11} \parallel\parallel \dot{e}_{11} \parallel + l_{12} \mid \varepsilon_{11} \mid) \\
\mid \Psi_2 \mid &\leq \frac{1}{1-\theta_2} \mid F_2(x) \mid + \frac{\theta_2}{1+\theta_2}(\parallel k_{11} \parallel\parallel e_{11} \parallel + \mid \varepsilon_{12} \mid + \\
&\quad \parallel k_{21} \parallel\parallel e_{21} \parallel + \parallel k_{22} \parallel\parallel e_{22} \parallel + \mid \varepsilon_{23} \mid) \\
\mid \dot{\Psi}_2 \mid &\leq \mid \dot{F}_2(x) \mid + \mid B_{21}(x) \mid\mid u_1 \mid + \mid B_{22}(x) \mid\mid u_2 \mid + \theta_2(\parallel k_{11} \parallel\parallel \dot{e}_{11} \parallel + \\
&\quad l_{12} \mid \varepsilon_{11} \mid + \parallel k_{21} \parallel\parallel \dot{e}_{21} \parallel + \parallel k_{22} \parallel\parallel \dot{e}_{22} \parallel + l_{23} \mid \varepsilon_{21} \mid)
\end{aligned}
$$

From the above equations, with consideration of the perturbation assumed as a smooth function of time, it can be concluded that the bound of perturbation and its derivative exist.

As a result, with both the **assumptions 1** and **2**, the effectiveness of such perturbation observer based control can be guaranteed.

4. Simulation Results

Simulation studies are carried out to verify the performance of the proposed HGO-NAC in comparing with the VC and ENO-NC. For simulation,

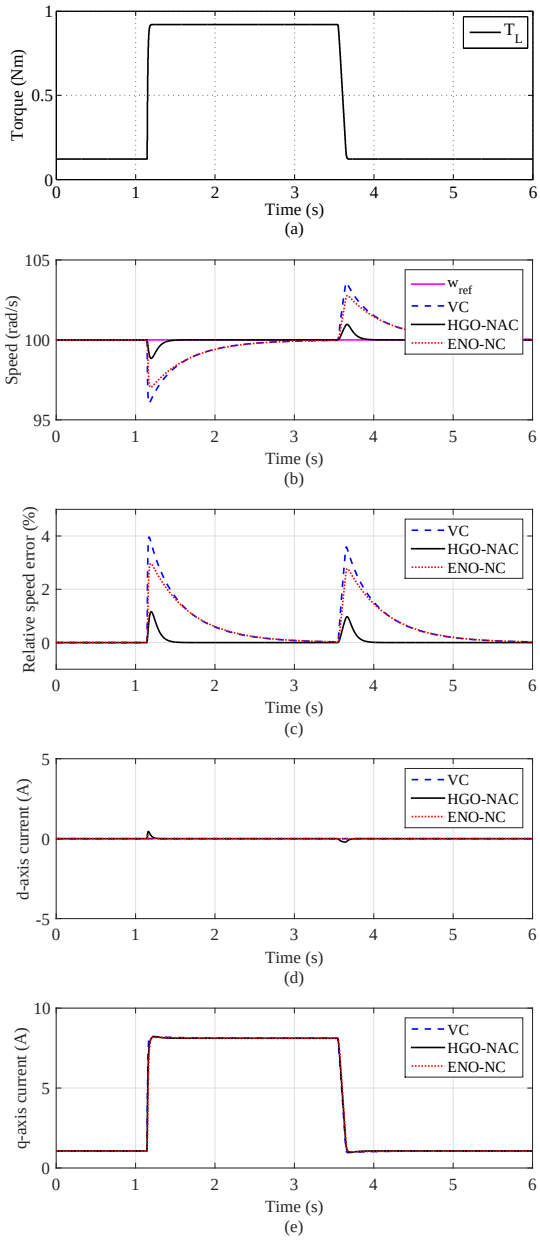

Figure 3: Simulation results of system responses to constant mechanical rotation speed with unknown step-change load torque disturbance. a) Load torque disturbance T_{L}; b) Mechanical rotation speed ω_{m}; c) Relative error of the ω_{m}; d) d-axis current i_{d}; e) q-axis current i_{q}.

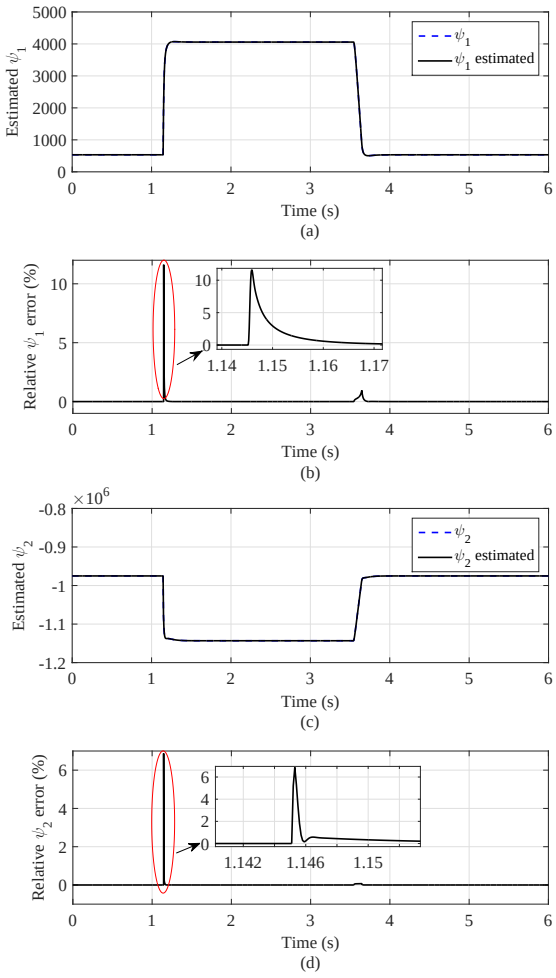

Figure 4: Estimations of system perturbations. a) Perturbation Ψ_1; b) Relative error of Ψ_1; c) Perturbation Ψ_2; d) Relative error of Ψ_2.

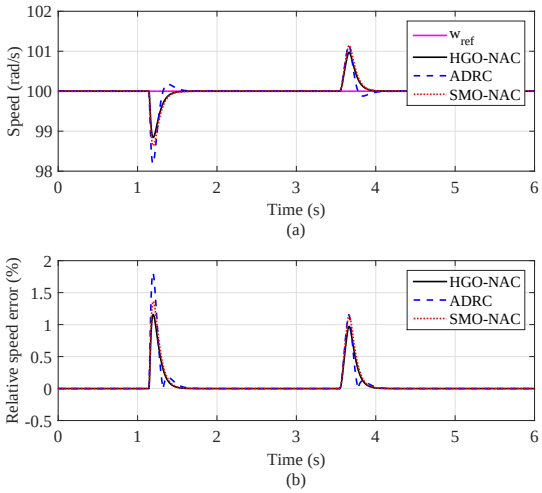

Figure 5: Simulation results of system responses to constant mechanical rotation speed with unknown step-change load torque disturbance under different observer based control methods. (a) Mechanical rotation speed ω_{m}; (b) Relative error of the ω_{m}.

the specifications of the PMSM supplied by MotorSolver are given as follows: rated power $P_{\mathrm{rated}} = 250$ W; rated current (RMS) $I_{\mathrm{rated}} = 5.7$ A; rated voltage $V_{\mathrm{rated}} = 42$ V; maximum speed $\omega_{\mathrm{max}} = 4000$ RPM; $p = 5$; $R_{\mathrm{s}} = 0.19$ Ω; $L_{\mathrm{d}} = L_{\mathrm{q}} = 0.49$ mH; $K_{\mathrm{e}} = 0.0151$ V.s/rad; $D = 2.6 \times 10^{-3}$ N.m.s/rad; $J = 1.23 \times 10^{-3}$ Kg.m^2.

Parameters of the HGO-NACs are designed based on pole-placement and listed in Table 1.

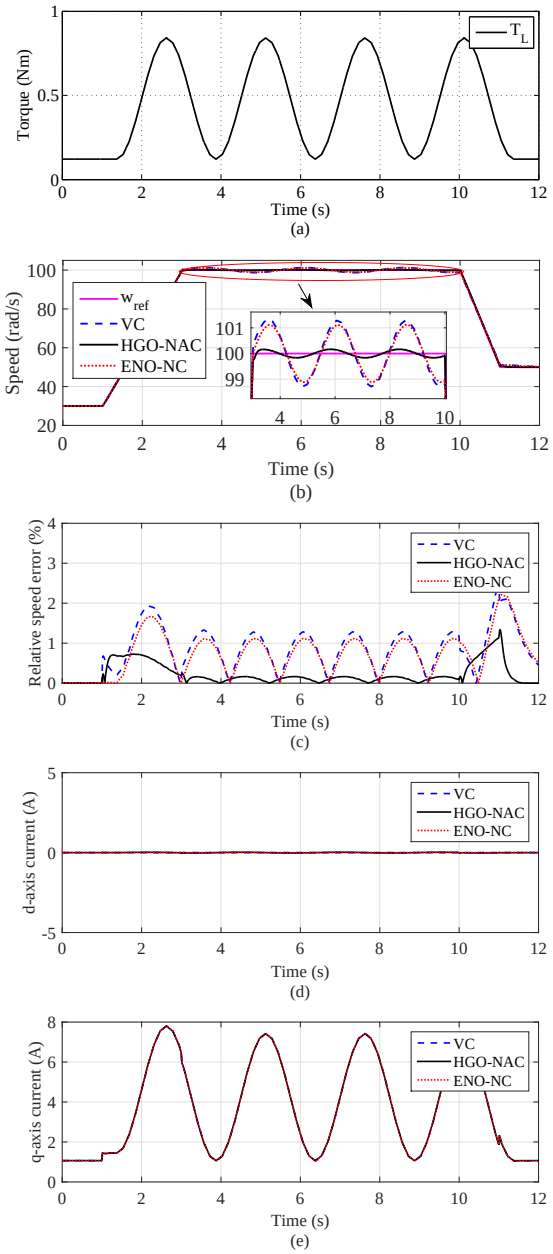

Figure 6: Simulation results of system responses to time-varying mechanical rotation speed with unknown time-varying load torque disturbance. a) Load torque disturbance T_{L}; b) Mechanical rotation speed ω_{m}; c) Relative error of the ω_{m}; d) d-axis current i_{d}; e) q-axis current i_{q}.

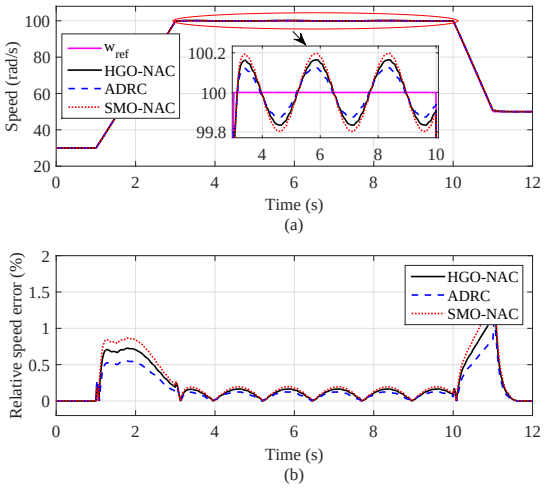

Figure 7: Simulation results of system responses to time-varying mechanical rotation speed with unknown time-varying load torque disturbance under different observer based control methods. (a) Mechanical rotation speed ω_{m}; (b) Relative error of the ω_{m}.

Table 1: Parameters of HGO-NAC schemes for simulation studies and experiment tests

Parameters of the HGPONAC-MPPT (25)	
Gains of observer (19)	$\alpha_{11} = 1.6 \times 10^2$, $\alpha_{12} = 6.4 \times 10^2$, $\epsilon_1 = 0.01$
Gains of observer (20)	$\alpha_{21} = 2.1 \times 10^2$, $\alpha_{22} = 1.47 \times 10^4$, $\alpha_{23} = 3.43 \times 10^5$, $\epsilon_2 = 0.01$
Gains of linear controller (24)	$k_{11} = 16$, $k_{21} = 4.84 \times 10^2$, $k_{22} = 4.4 \times 10^1$

4.1. Scenario I: Constant Mechanical Rotation Speed with Unknown Step-Change Load Torque Disturbance

In this Sub-section, the unknown step-change load torque disturbance and constant mechanical rotation speed are applied. It is to verify the robustness of the control system against unknown load torque disturbance.

The unknown step-change load torque disturbance T_{L} and mechanical

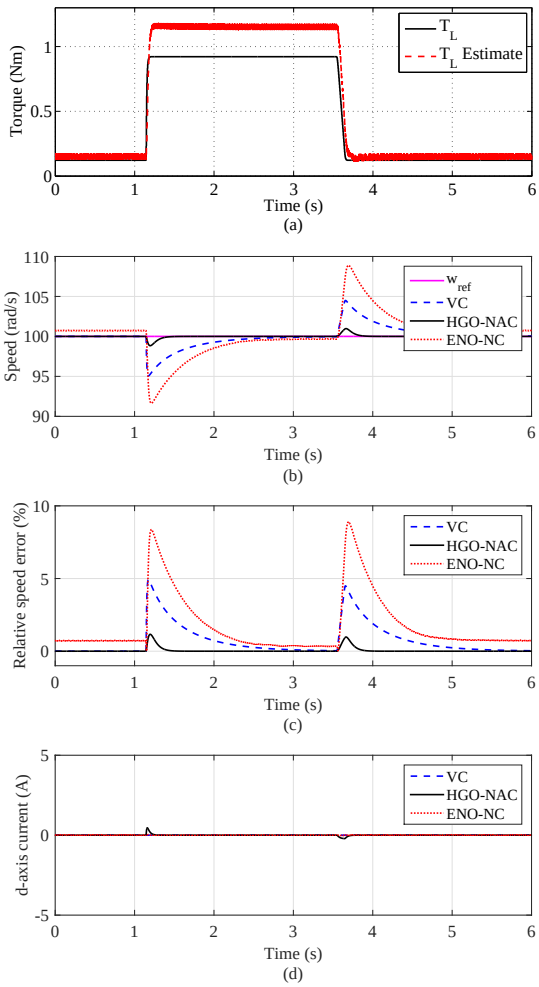

Figure 8: Simulation results of system responses to constant mechanical rotation speed with unknown step-change load torque disturbance and field flux variation. a) Load torque disturbance T_{L}; b) Mechanical rotation speed ω_{m}; c) Relative error of the ω_{m}; d) d-axis current i_{d}.

rotation speed reference ω_{ref} are shown in Fig. 3(a) and (b), respectively. It can be seen from Fig. 3(b) and (c) that, the HGO-NAC can achieve the best tracking performance of the mechanical rotation speed ω_{m} with unknown step-change load torque disturbance T_{L}. The maximum relative error ($|\frac{\omega_{\mathrm{m}}-\omega_{\mathrm{ref}}}{\omega_{\mathrm{ref}}}| \times 100\%$) is approximately 4% and 3% under the VC and ENO-NC, respectively. It is because that the VC cannot deal with the unknown load torque disturbance caused by load torque variation and the ENO-NC cannot provide high tracking performance under the fast varying load torque disturbance as mentioned in (Solsona, Valla and Muravchik, 2000). Although the performance of the HGO-NAC is slightly impacted by the unknown step-change load torque disturbance, the maximum relative error ($|\frac{\omega_{\mathrm{m}}-\omega_{\mathrm{ref}}}{\omega_{\mathrm{ref}}}| \times 100\%$) is approximately 1%. The d-axis current i_{d} response is shown in Fig. 3(d). The q-axis current i_{q} response is shown in Fig. 3(e). It can be found that the VC, ENO-NC and HGO-NAC can always keep the i_{d} around 0. In addition, the performances of these three control methods through maximum regulation error and integral of the time multiplied by the absolute error (ITAE) are shown in Table 2.

As mentioned in previous section, the main advantage of the proposed HGO-NAC is achieved by estimating the defined perturbation terms (14),

Table 2: Simulation results: control performance indices comparison in ITAE and maximum error under different scenarios

Scenario no.	VC		ENO-NC		HGO-NAC		SMO-NAC		ADRC	
	ITAE	error	ITAE	error	ITAE	error	ITAE	error	ITAE	error
I	3.49	3.96	3.17	2.97	0.30	1.16	0.36	1.37	0.34	1.81
II	8.53	1.43	7.48	1.25	2.08	0.69	2.36	0.76	1.50	0.54

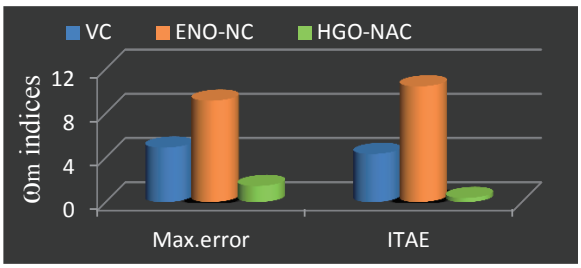

Figure 9: Control performance indices comparison in maximum error and ITAE under field flux variation:ω_{m} indices.

through the perturbation observers (19) and (20). The real values of perturbations and the estimated values provided by observers are compared in Fig. 4. It can be found that the observers can accurately estimate the perturbations.

In addition, the comparison among the proposed HGO-NAC, sliding-mode states and perturbation observer based NAC (SMO-NAC) in (Jiang and Wu, 2002), and nonlinear SPO based active disturbance rejection control (ADRC) in (Han, 2009) under this scenario are shown in Fig. 5 and Table 2. The mechanical rotation speed response under different observer based controllers is shown in Fig. 5(a) and (b). The results of Table 2 show

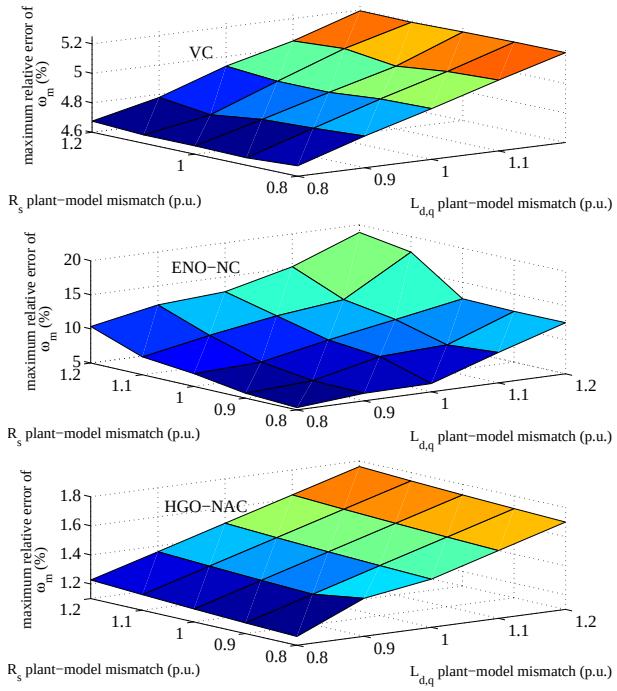

Figure 10: Maximum relative error of ω_{m} obtained under constant mechanical rotation speed with unknown step-change load torque disturbance for plant-model mismatches:stator resistance R_{s} and inductance $L_{\mathrm{d,q}}$ vary between 0.8 and 1.2 p.u., and filed flux K_{e} decreases to 80% of nominal value.

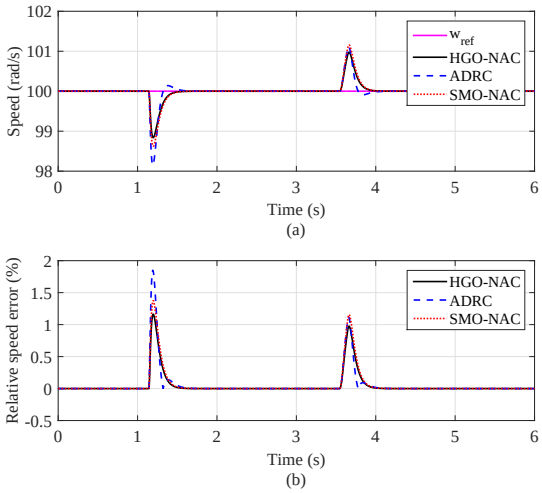

Figure 11: Simulation results of system responses to constant mechanical rotation speed with unknown step-change load torque disturbance and all system parameters decreasing from their nominal values to 80% of nominal values under different observer based control methods. a) Mechanical rotation speed ω_{m}; b) Relative error of the ω_{m}.

that the control performances of different observer based control methods are similar in the maximum regulation error and ITAE, but the HGO is simple in structure, gain tuning and stability analysis.

4.2. Scenario II: Time-Varying Mechanical Rotation Speed With Unknown Time-Varying Load Torque Disturbance

In this Sub-section, the unknown time-varying load torque disturbance and time-varying mechanical rotation speed are applied. It is to verify the robustness against load torque disturbance and dynamic performance of the control system.

Fig. 6 shows the responses of the PMSM for the case of time-varying mechanical rotation speed with unknown time-varying load torque disturbance. It can be found from Fig. 6 and Table 2 that, the HGO-NAC achieves satisfactory tracking performances of the ω_{m} and i_{d}, and provides high robustness against load torque disturbance. When the ω_{m} and T_{L} vary at the same time, the tracking performance of the ω_{m} is approximately 2.5% and 2.3% maximum relative error ($|\frac{\omega_{\mathrm{m}}-\omega_{\mathrm{ref}}}{\omega_{\mathrm{ref}}}| \times 100\%$) under the VC and ENO-NC, respectively.

The comparison among the HGO-NAC, SMO-NAC and ADRC under this scenario are shown in Fig. 7 and Table 2. It can be seen that all these three observer based control methods provide satisfactory performances and high robustness against time-varying load torque disturbance.

4.3. Scenario III: Robustness Against Parameter Uncertainties

In this Sub-section, parameter uncertainty tests have been done, which are mainly to verify the robustness of the control system against parameter variations.

For a practical PMSM system, its system parameter values may vary due to magnetic saturation, operating temperature, and manufacturing tolerance. Hence, the currently actual parameters and the nominal ones given by the

manufacturer may possibly exist a gap. The control performances of different control methods are tested under the parameter uncertainties. Note that the given unknown step-change load torque disturbance and reference mechanical rotation speed are the same as Scenario I in the following simulation study cases.

The mismatch of various parameters are simulated. The results for the mismatch of field flux K_{e} decreasing from its nominal value to 80% of nominal value are given. The results under the proposed HGO-NAC, ENO-NC and VC are given. It can be seen, from Fig. 8 that, the proposed HGO-NAC achieves the best dynamic performance, while the ENO-NC achieves the worse dynamic performance than the VC. The load torque disturbance cannot be well estimated under the ENO-NC, and the mechanical rotation speed is with steady state speed error under the ENO-NC. It is because that the flux variation may result in steady state speed error as reported in (Solsona, Valla and Muravchik, 2000). Fig. 9 shows performance of different control methods through maximum relative error of ω_{m} and ITAE. The results of Fig. 9 also show the proposed HGO-NAC is most insensitive to flux variation.

In Fig. 10, a series of plant-model mismatches of stator resistance R_s and

inductance $L_{\mathrm{d,q}}$ with $\pm 20\%$ variations around their nominal value, and filed flux K_{e} decreasing to 80% of nominal value are undertaken. The maximum relative error of ω_{m} is recorded for a clear comparison. Fig. 10 shows that the maximum relative error of ω_{m} obtained by VC, ENO-NC and HGO-NAC is around 5.2%, 18% and 1.7%, respectively. This can be explained as follows, the proposed HGO-NAC estimates all uncertainties and does not need the accurate system parameters. Thus, it has better robustness than ENO-NC which requires accurate system parameters.

The HGO-NAC, SMO-NAC and ADRC are used for comparison of control performance when all system parameters decrease from their nominal values to 80% of nominal values. It can be seen from Figs. 11 and 12 that, all these three observer control schemes not only achieve satisfactory dynamic performance, but also have high robustness against parameter variations and load torque disturbance.

5. Experimental Results

To further verify the effectiveness of the proposed HGO-NAC method, the experimental tests have been done. The experimental tests and simulation studies use the same set of the PMSM system parameters and controller

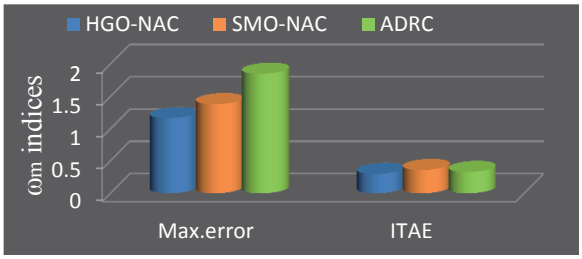

Figure 12: Control performance indices comparison in maximum error and ITAE under system parameter variations:ω_{m} indices.

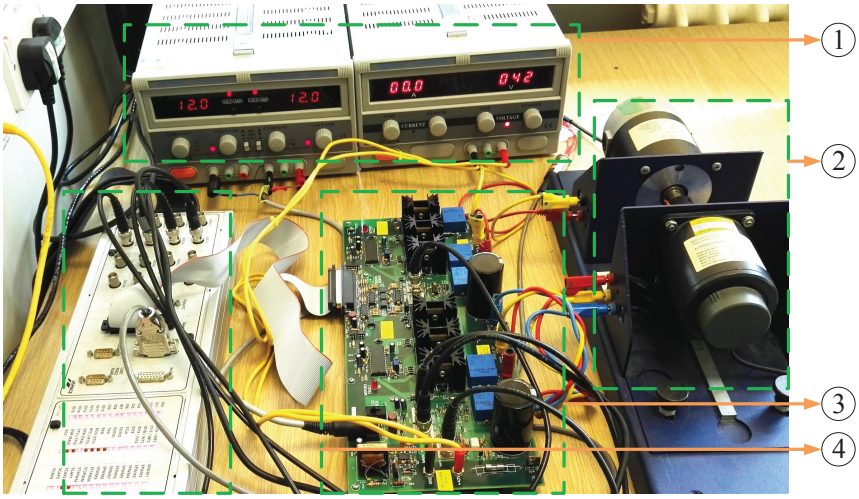

Figure 13: Experimental setup

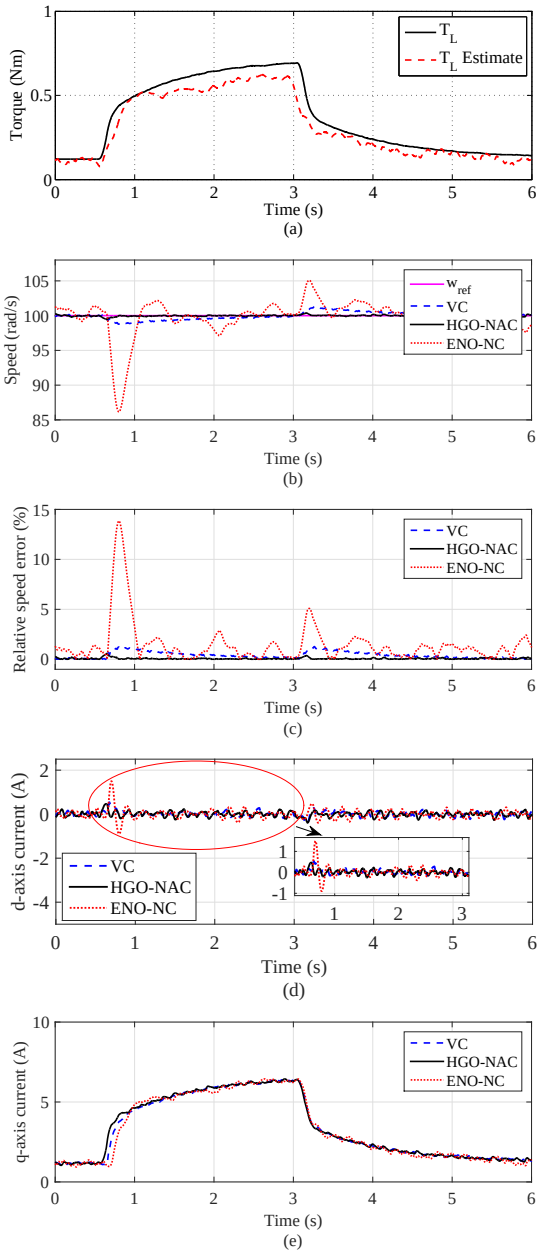

Figure 14: Experimental results of system responses to constant mechanical rotation speed 100 rad/s with unknown step-change load torque disturbance. a) Load torque disturbance T_{L}; b) Mechanical rotation speed ω_{m}; c) Relative error of the ω_{m}; d) d-axis current i_{d}; e) q-axis current i_{q}.

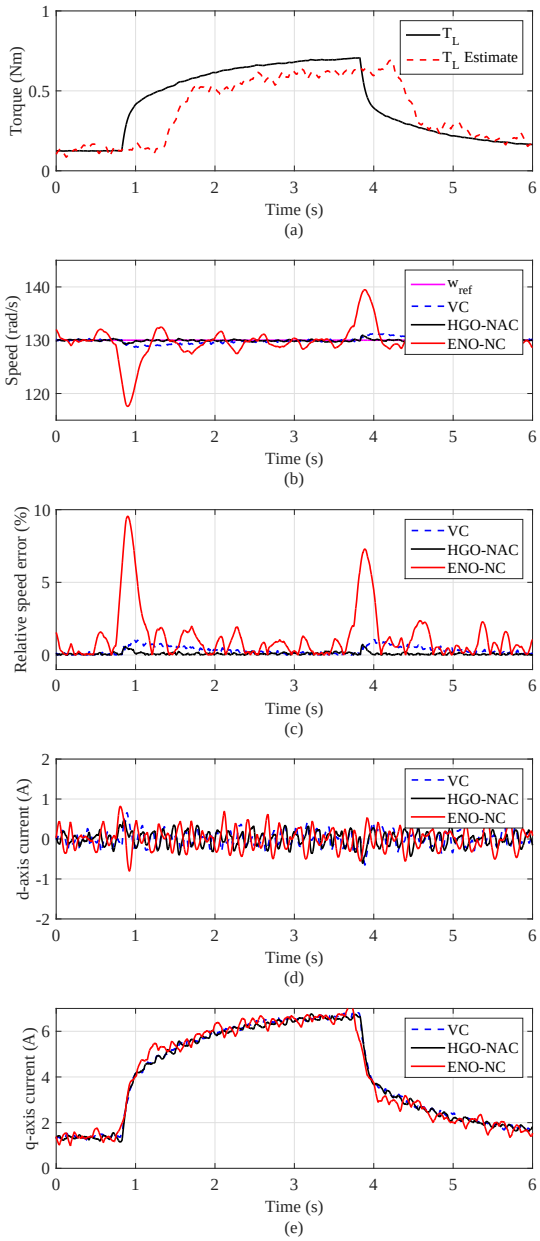

Figure 15: Experimental results of system responses to constant mechanical rotation speed 130 rad/s (1241 rpm) with unknown step-change load torque disturbance. a) Load torque disturbance T_{L}; b) Mechanical rotation speed ω_{m}; c) Relative error of the ω_{m}; d) d-axis current i_{d}; e) q-axis current i_{q}.

parameters. In hardware implementation, the PMSM to be controlled is a 5 pole pairs, 250 W PMSM with rated 42 V input and 5.7 A RMS current and supplied by MotorSolver. It is coupled with a DC motor, which is used to produce load torque disturbance for the PMSM. Both the PMSM and DC motor are drived by an IGBT-based inverter, which is controlled by PWM signal produced by DS1104 dSPACE processor board. The dSPACE software can compile the Simulink control loop to C-code by using MATLAB/Simulink real-time workshop (RTW) before being downloaded to DS1104 dSPACE processor board. The dSPACE processor board is also used to receive the mechanical rotation speed and position measured by an incremental optical 1000-line encoder, which is synchronized with the motor shaft. In addition, the measured results of motor states are displayed on the dSPACE control desk, and both the reference control targets and controller parameters can be adjusted in real time.

5.1. Scenario I: Constant Mechanical Rotation Speed With Unknown Step-Change Load Torque Disturbance

This Sub-section is to verify the robustness against unknown step-change load torque disturbance. Fig. 14 shows the experimental results. In the

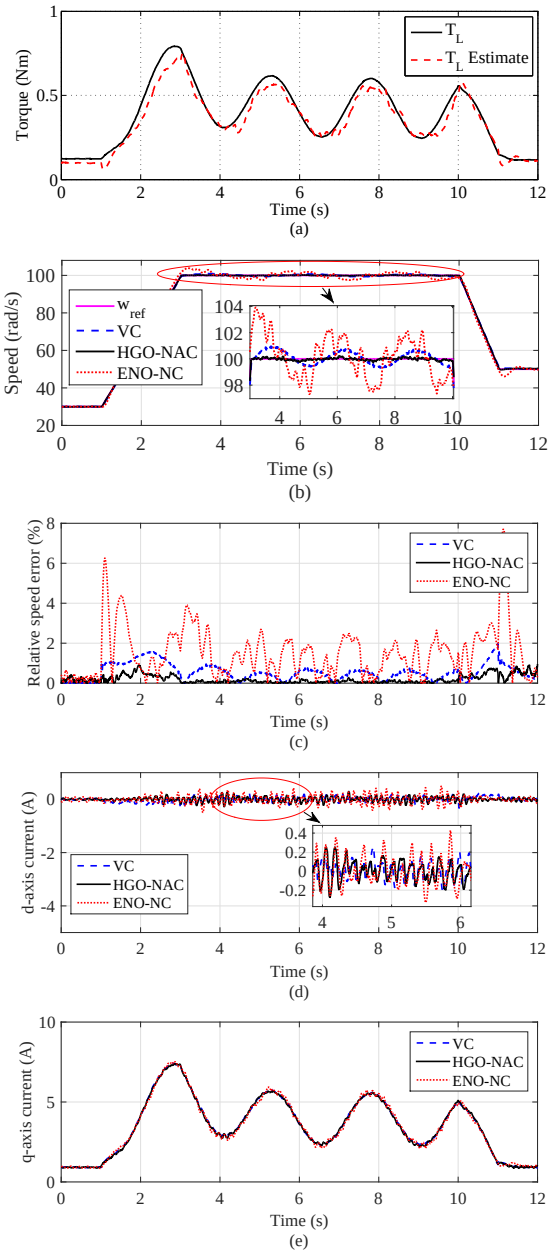

Figure 16: Experimental results of system responses to time-varying mechanical rotation speed with unknown time-varying load torque disturbance. a) Load torque disturbance T_{L}; b) Mechanical rotation speed ω_{m}; c) Relative error of the ω_{m}; d) d-axis current i_{d}; e) q-axis current i_{q}.

experiment, the unknown load torque disturbance T_{L} is provided by the DC motor, which is different from the load torque disturbance shown in Fig. 3(a). Fig. 14(a) and (b) shows the unknown step-change load torque disturbance T_{L} and mechanical rotation speed reference ω_{ref}, respectively. The mechanical rotation speed ω_{m} and its relative error ($|\frac{\omega_{\mathrm{m}}-\omega_{\mathrm{ref}}}{\omega_{\mathrm{ref}}}| \times 100\%$) are shown in Fig. 14(b) and (c), respectively. Fig. 14(d) and (e) shows the d,q-axis current $i_{\mathrm{d,q}}$. According to Fig. 14 and Table 3, it can be seen that the proposed HGO-NAC achieves the best dynamic performance. The ENO-NC provides the worst dynamic performance not as the that achieved by the VC in the simulation tests. In experimental tests, the PMSM parameters are from PMSM nameplate. However, the motor parameter variations generate output inaccuracies as a function of build, life, and experiment environment variations, therefore the real electrical parameters used in the experiment may not be the same as the nameplate. The ENO-NC requires the accurate electrical parameters. The electrical parameter variations give rise to a steady state speed error and may compromise the stability of the whole system as reported in (Solsona, Valla and Muravchik, 2000). Fig. 14(a) shows that the unknown load torque disturbance cannot be exactly estimated by the ENO-NC with electrical parameter variations. This may result in that

the ENO-NC achieves a worse performance than the VC. In Fig. 15, the mechanical rotation speed increases from 100 rad/s (955 rpm) to 130 rad/s (1241 rpm)and the load torque disturbance is the same as that shown in Fig. 14(a). The proposed HGO-NAC and ENO-NC achieve the best and worst dynamic performances, respectively.

5.2. Scenario II: Time-Varying Mechanical Rotation Speed Under Unknown Time-Varying Load Torque Disturbance

This Sub-section is not only verify the robustness against unknown time-varying load torque disturbance, but also dynamic performance of the control system under time-varying mechanical rotation speed. In this experimental test case, the applied time-varying load torque disturbance T_{L} and reference mechanical rotation speed ω_{ref} are shown in Fig. 16(a) and (b), respectively. Compared with the VC and ENO-NC, the HGO-NAC has higher robustness against unknown time-varying load torque disturbance shown in Fig. 16 and Table 3.

Table 3: Experimental results: control performance indices comparison in ITAE and maximum error under different scenarios.

Scenario no.	**VC**		**ENO-NC**		**HGO-NAC**	
	ITAE	**error**	**ITAE**	**error**	**ITAE**	**error**
I	2.45	1.27	8.92	13.86	0.48	0.38
II	5.17	1.18	14.655	3.92	1.63	0.60
III	5.05	2.92	7.17	5.86	0.96	0.93

5.3. Scenario III: Constant Mechanical Rotation Speed With Unknown Step-Change Load Torque Disturbance Under Parameter Uncertainties

To further evaluate the effectiveness of the proposed control strategy, the parameter uncertainty test has been done. Meanwhile, the unknown load torque and mechanical rotation speed as the same as Scenario I are applied. Based on (Jung, Leu, Do, Kim and Choi, 2015), it is assumed that R_{s}, $L_{\mathrm{d,q}}$ and J are changed as $+70\%$, -30% and $+120\%$, respectively. In addition, the field flux K_{e} is assumed to decrease to its 80% of nominal value. Notice that it is not easy to directly change the motor parameters in experiment tests. Therefore, the changes of the system parameters in the control scheme have been done.

It can be seen from Fig. 17 that, the mechanical rotation speed under the ENO-NC can not be kept at steady state when the load torque disturbance can not be well estimated. It is because that the load torque observer requires

the accurate system parameters. Fig. 17 and Table 3 show that the VC can provide better performance than the ENO-NC. However, its performance is still affected under parameter variations. Comparing with Scenario I and III, the ITAE and maximum error increase from 2.45% to 5.05% and 1.27% to 2.92%, respectively. Compared with the VC and ENO-NC, the proposed HGO-NAC provides much less recovery time and smaller error of mechanical rotation speed. The proposed HGO-NAC can achieve high-performance with load torque disturbance and parameter uncertainties.

6. Conclusion

An HGO-NAC strategy has been proposed for controlling the speed of the PMSM driving unknown time-varying load torque disturbance. In the proposed HGO-NAC, all possibly unknown and time-varying dynamics of the PMSM, such as system parameter uncertainties, unknown nonlinearities and load torque disturbance of the PMSM, are included in lumped perturbation terms, which are estimated by states and perturbation observers. The real-time estimates of perturbation are employed to compensate the real perturbation for fully linearizing the PMSM system. Compared with the VC tuned around a specific operating point, the HGO-NAC can provide glob-

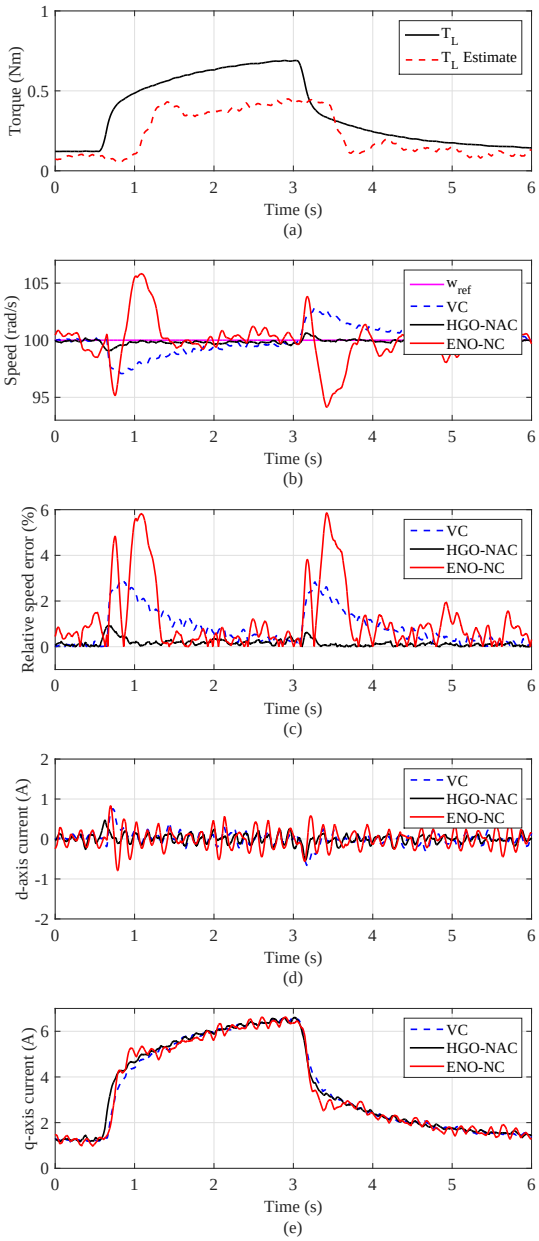

Figure 17: Experimental results of system responses to constant mechanical rotation speed with unknown step-change load torque disturbance under parameter uncertainties. a) Load torque disturbance T_{L}; b) Mechanical rotation speed ω_{m}; c) Relative error of the ω_{m}; d) d-axis current i_{d}e) q-axis current i_{q}.

al optimal performance across the whole operation region. The HGO-NAC has better robustness than the ENO-NC under fast varying load torque disturbance and parameter uncertainties. Compared with both the ENO-NC and VC, simulation and experimental results have shown that, the proposed HGO-NAC always achieves highest performance under different operation conditions and provides best robustness in the presence of parameter uncertainties and unknown fast varying load torque disturbance. Further studies will focus on speed sensorless control strategy for reducing the cost of the system.

Acknowledgements

This work is supported by National Natural Science Foundation of China under Grant No. 51577075.

Alsumiri, M., Li, L. Y., Jiang, L., and Tang, W. H. (2018). Residue Theorem based soft sliding mode control for wind power generation systems. *Protection and Control of Modern Power Systems*, *3*(3), 247-258.

Bifaretti S., Iacovone V., Rocchi A., Tomei P., and Verrelli C. M., (2012) Nonlinear speed tracking control for sensorless PMSMs with unknown load

torque: From theory to practice, *Control Engineering Practice*, *20*(7), 714-724.

Chai S., Wang L. P., and Rogers E., (2013) Model predictive control of a permanent magnet synchronous motor with experimental validation, *Control Engineering Practice*, *21*(11), 1584-1593.

Chaoui H., Khayamy M., and Aljarboua A. A., (2017) Adaptive interval type-2 fuzzy logic control for pmsm drives with a modified reference frame, *IEEE Transactions on Industrial Electronics*, *64*(5), 3786-3797.

Chen J., Jiang L., Yao Wei, and Wu Q. H., (2014) Perturbation estimation based nonlinear adaptive control of a full-rated converter wind-turbine for fault ride-through capability enhancement, *IEEE Transactions on Power Systems*, *29*(6), 2733-2743.

Cheng S. and Li C. W., (2011) Fuzzy PDFF-IIR controller for PMSM drive systems, *Control Engineering Practice*, *19*(8), 828-835.

Choi H. H. and Jung J. -W., (2013) Discrete-time fuzzy speed regulator design for PM synchronous motor, *IEEE Transactions on Industrial Electronics*, *60*(2), 600-607.

Choi H. H., Yun H. M., and Kim Y., (2015) Implementation of evolutionary fuzzy pid speed controller for pm synchronous motor, *IEEE Transactions on Industrial Informatics*, *11*(2), 540-547.

Elmas C., and Ustun O., (2008) A hybrid controller for the speed control of a permanent magnet synchronous motor drive, *Control Engineering Practice*, *16*(3), 260-270.

El-Sousy F. F. M., (2013) Intelligent optimal recurrent wavelet elman neural network control system for permanent-magnet synchronous motor servo drive, *IEEE Transactions on Industrial Informatics*, *9*(4), 1986-2003.

Feng Y., Yu X. H., and Han F. L., (2013) High-order terminal sliding-mode observer for parameter estimation of a permanent-magnet synchronous motor, *IEEE Transactions on Industrial Electronics*, *60*(10), 4272-4280.

Hamida M. A., Leon J. D., and Glumineau A., (2017) Experimental sensorless control for IPMSM by using integral backstepping strategy and adaptive high gain observer, *Control Engineering Practice*, *59*, 64-76.

Han J. Q., (2009) From PID to active disturbance rejection control, *IEEE Transactions on Industrial Electronics*, *56*(3), 900-906.

Jiang L. and Wu Q. H., (2002) Nonlinear adaptive control via sliding-mode state and perturbation observer, *IEE Proceedings - Control Theory and Applications*, *149*(4), 269-277.

Jiang L., Wu Q. H., and Wen J. Y., (2004) Decentralized nonlinear adaptive control for multimachine power systems via high-gain perturbation observer, *IEEE Transactions on Circuits and Systems I: Regular Papers*, *51*(10), 2052-2059.

Jiang Y. J., Xu W., Mu C. X., and Liu Y., (2018) Improved deadbeat predictive current control combined sliding mode strategy for pmsm drive system, *IEEE Transactions on Vehicular Technology*, *67*(1), 251-263.

Jung J. -W., Leu V. Q., Do T. D., E. -K. Kim, and Choi H. H., (2015) Adaptive PID speed control design for permanent magnet synchronous motor drives, *IEEE Transactions on Power Electronics*, *30*(2), 900-908.

Khanchoul M., Hilairet M., and Normand-Cyrot D., (2014) A passivity-based controller under low sampling for speed control of PMSM, *Control Engineering Practice*, *26*, 20-27.

Kim H., Son J., and Lee J., (2011) A high-speed sliding-mode observer for

the sensorless speed control of a PMSM, *IEEE Transactions on Industrial Electronics*, *58*(9), 4069-4077.

Kim K. -H. and Youn M. -J., (2002) A nonlinear speed control for a PM synchronous motor using a simple disturbance estimation technique, *IEEE Transactions on Industrial Electronics*, *49*(3), 524-535.

Kim S. -K, (2017) Robust adaptive speed regulator with self-tuning law for surfaced-mounted permanent magnet synchronous motor, *Control Engineering Practice*, *61*, 55-71.

Kim S. -K., Lee J. -S., and Lee K. -B., (2016) Offset-free robust adaptive back-stepping speed control for uncertain permanent magnet synchronous motor, *IEEE Transactions on Power Electronics*, *31*(10), 7065-7076.

Krishnan R., (2001) Electric Motor Drives: Modeling, Analysis, and Control, Prentice-Hall, New Jersey.

Lee T. S., Lin C. H., and Lin F. J., (2005) An adaptive H controller design for permanent magnet synchronous motor drives, *Control Engineering Practice*, *13*(4), 425-439.

Leu V. Q., Choi H. H., and Jung J. W., (2012) Fuzzy sliding mode speed

controller for PM synchronous motors with a load torque observer, *IEEE Transactions on Power Electronics*, *27*(3), 1530-1539.

Li S. H. and Liu Z. G., (2009) Adaptive speed control for permanent-magnet synchronous motor system with variations of load inertia, *IEEE Transactions on Industrial Electronics*, *56*(8), 3050-3059.

Li S. H., Zhou M. M., and Yu X. H., (2013) Design and implementation of terminal sliding mode control method for pmsm speed regulation system, *IEEE Transactions on Industrial Informatics*, *9*(4), 1879-1891.

Lin C. -K., Liu T. -H., and Yang S. -H., (2008) Nonlinear position controller design with input-output linearisation technique for an interior permanent magnet synchronous motor control system, *IET Electric Power Applications*, *1*(9), 14-26.

Linares-Flores J., Garcia-Rodriguez C., Sira-Ramirez H., and Ramirez-Cardenas O. D., (2015) Robust backstepping tracking controller for low speed PMSM positioning system: Design, analysis, and implementation, *IEEE Transactions on Industrial Informatics*, *11*(5), 1130-1141.

Liu H. X. and Li S. H., (2012) Speed control for PMSM servo system using

predictive functional control and extended state observer, *IEEE Transactions on Industrial Electronics*, *59*(2), 1171-1183.

Liu K. and Zhu Z. Q., (2014) Online estimation of the rotor flux linkage and voltage-source inverter nonlinearity in permanent magnet synchronous machine drives, *IEEE Transactions on Power Electronics*, *29*(1), 418-427.

Lu Y. S, (2008) Smooth speed control of motor drives with asymptotic disturbance compensation, *Control Engineering Practice*, *16*(5), 597-608.

Luo Y., Chen Y. Q., Ahn H. S., and Pi Y. G., (2010) Fractional order robust control for cogging effect compensation in PMSM position servo systems: Stability analysis and experiments, *Control Engineering Practice*, *18*(9), 1022-1036.

Ma Z. X., Saeidi S., and Kennel R., (2014) FPGA implementation of model predictive control with constant switching frequency for pmsm drives, *IEEE Transactions on Industrial Informatics*, *10*(4), 2055-2063.

Mohamed Y. A. -R. I., (2007) Design and implementation of a robust current-control scheme for a PMSM vector drive with a simple adaptive disturbance observer, *IEEE Transactions on Industrial Electronics*, *54*(4), 1981-1988.

Morawiec M., (2013) The adaptive backstepping control of permanent magnet synchronous motor supplied by current source inverter, *IEEE Transactions on Industrial Informatics*, *9*(2), 1047-1055.

Niu X. T., Zhang C. L., and Li H., (2017) Active disturbance attenuation control for permanent magnet synchronous motor via feedback domination and disturbance observer, *IET Control Theory and Applications*, *11*(6), 807-815.

Preindl M. and Bolognani S., (2013) Model predictive direct torque control with finite control set for pmsm drive systems, part 1: maximum torque per ampere operation, *IEEE Transactions on Industrial Informatics*, *9*(4), 1912-1921.

Sira-ramirez H., Linares-Flores J., Garcia-Rodriguez C., and Contreras-Ordaz M. A., (2014) On the control of the permanent magnet synchronous motor: An active disturbance rejection control approach, *IEEE Transactions on Control Systems Technology*, *22*(5), 2056-2063.

Solsona J., Valla M. I., and Muravchik C., (1996) A nonlinear reduced order observer for permanent magnet synchronous motors, *IEEE Transactions on Industrial Electronics*, *43*(4), 492-497.

Solsona J., Valla M. I., and Muravchik C., (2000) Nonlinear control of a permanent magnet synchronous motor with disturbance torque estimation, *IEEE Transactions on Energy Conversion*, *15*(2), 163-168.

Son Y. I., Kim I. H., Choi D. S., and Shim H., (2015) Robust cascade control of electric motor drives using dual reduced-order PI observer, *IEEE Transactions on Industrial Electronics*, *62*(6), 3672-3682.

Su Y. X., Zheng C. H., and Duan B. Y., (2005) Automatic disturbances rejection controller for precise motion control of permanent-magnet synchronous motors, *IEEE Transactions on Industrial Electronics*, *52*(3), 814-823.

Tami R., Boutat D., Zheng G., Kratz F., and Gouri R. E., (2017) Rotor speed, load torque and parameters estimations of a permanent magnet synchronous motor using extended observer forms, *IET Control Theory and Applications*, *11*(9), 1485-1492.

Underwood S. J. and Hussain I., (2010) Online parameter estimation and adaptive control of permanent-magnet synchronous machines, *IEEE Transactions on Industrial Electronics*, *57*(7), 2435-2443.

Verrelli C. M., Tomei P., Lorenzani E., Migliazza G., and Immovilli F., (2017)

Nonlinear tracking control for sensorless permanent magnet synchronous motors with uncertainties, *Control Engineering Practice*, *60*, 157-170.

Wu Q. H., Jiang L., and Wen J. Y., (2004) Decentralized adaptive control of interconnected non-linear systems using high gain observer, *International Journal of Control*, *77*(8), 703-712.

Xu W., Jiang Y. J., and Mu C. X., (2016) Novel composite sliding mode control for pmsm drive system based on disturbance observer, *IEEE Transactions on Applied Superconductivity*, *26*(7), 1-5.

Yan Y. D., Yang J., Sun Z. X., Zhang C. L., Li S. H., and Yu H. Y., (2018) Robust speed regulation for pmsm servo system with multiple sources of disturbances via an augmented disturbance observer, *IEEE/ASME Transactions on Mechatronics*, *23*(2), 769-780.

Yang B., Jiang L., Yao W., and Wu Q. H., (2015) Perturbation estimation based coordinated adaptive passive control for multimachine power systems, *Control Engineering Practice*, *44*, 172-192.

Yang B., Yu T., Shu H. C., Dong J., and Jiang L., (2018) Robust sliding-mode control of wind energy conversion systems for optimal power extraction via nonlinear perturbation observers, *Applied Energy*, *210*, 711-723.

Yand B., Yu T., Shu H. C., Zhang Y. M., Chen J., Sang Y. Y., and Jiang L., (2018) Passivity-based sliding-mode control design for optimal power extraction of a PMSG based variable speed wind turbine, *Renewable Energy*, *119*, 577-589.

Yang H. T., Zhang Y. C., Liang J. J. Y., Xia B., Walker P. D., and Zhang N., (2018) Deadbeat control based on a multipurpose disturbance observer for permanent magnet synchronous motors, *IET Electric Power Applications*, *12*(5), 708-716.

Yang J., Chen W. H., Li S. H., Guo L., and Yan Y. D., (2017) Disturbance/Uncertainty estimation and attenuation techniques in PMSM drives-a survey, *IEEE Transactions on Industrial Electronics*, *64*(4), 3273-3285.

Youcef K., and Wu S., (1992) Input/output linearization using time delay control, *Journal of Dynamic Systems, Measurement, and Control*, *114*(1), 10-19.

Zhang X. G., Hou B. S., and Mei Y., (2017) Deadbeat predictive current control of permanent-magnet synchronous motors with stator current

and disturbance observer, *IEEE Transactions on Power Electronics*, *32*(5), 3818-3834.

Zhang X. G. and Li Z. X., (2017) Sliding-Mode observer-based mechanical parameter estimation for permanent magnet synchronous motor, *IEEE Transactions on Power Electronics*, *31*(8), 5732-5745.

Zhang X. G., Sun L. Z., Zhao K., and Sun L., (2013) Nonlinear speed control for pmsm system using sliding-mode control and disturbance compensation techniques, *IEEE Transactions on Power Electronics*, *28*(3), 1358-1365.

Zhou J. G. and Wang. Y. Y., (2005) Real-time nonlinear adaptive back-stepping speed control for a PM synchronous motor, *Control Engineering Practice*, *13*(10), 1259-1269.

Zhu G. C., Dessaint L. A., Akhrif Q., and Kaddouri A., (2000) Speed tracking control of a permanent-magnet synchronous motor with state and load torque observer, *IEEE Transactions on Industrial Electronics*, *47*(2), 346-355.